Seasonal flow types of glaciers in Sermilik Fjord, Greenland, over 2016–2021

K. Poinar[1,2]

[1]Department of Geology, University at Buffalo, Buffalo, NY 14260, USA
[2]RENEW Institute, University at Buffalo, Buffalo, NY 14260, USA

Key Points:

- Glacier type varies across Sermilik Fjord: Helheim is terminus-driven, Fenris and Midgard are runoff-adapting, Pourquoi-Pas is runoff-driven
- Decomposition by empirical orthogonal functions and principal components reveals glacier type using data at all points in the glacier domain
- Inferred glacier types differ slightly from previous work because we isolate the seasonal component and weight all locations equally

This paper is a preprint submitted to EarthArXiv. It has not yet been peer reviewed.

As of September 2022, it is in review at the Journal of Geophysical Research: Earth Surface.

Corresponding author: K. Poinar, `kpoinar@buffalo.edu`

Abstract

Greenland glaciers have three primary seasonal ice flow patterns, or "types": terminus driven, runoff driven, and runoff adapting. To date, glacier types have been identified by analyzing flow at a single location near the terminus; information at all other locations is discarded. Here, we use principal component (PC) / empirical orthogonal function (EOF) analysis to decompose multi-year time series of glacier speed, combined from three satellite-derived products at four glaciers feeding Sermilik Fjord, Greenland. This improves on single-point methods by yielding temporal patterns (PCs), which allow identification of glacier type, and associated spatial patterns (EOFs), which ensure the result reflects data at all locations on the glacier. We find that the leading mode is uniformly signed over the entire glacier domain, that this mode explains the majority of the variance in speed, and therefore that glacier type can be inferred from the leading PC. We find that Helheim Glacier was terminus-driven, Fenris Glacier and Midgard Glacier were runoff-adapting, and Pourquoi-Pas Glacier was runoff-driven over 2016-2021. Our classification agrees with previous work for Helheim and Midgard Glaciers, but differs at the other two. At all but Fenris Glacier, the leading PC correlates significantly with the speed pattern observed at the single point used in previous analyses. Thus, Fenris Glacier has more complex flow patterns than single-point analysis can capture, and wider spatial analysis techniques such as EOF/PC are required. We suggest that, due to its low computational cost and inclusion in standard analysis packages, EOF/PC analysis should be used for assessing glacier type.

Plain Language Summary

Glaciers change their flow speed throughout the year. Most glaciers move slowest in winter and more quickly during summer, but subtle differences in the timing give us clues as to what controls the speed of the glacier. Some glaciers respond to ocean conditions ("terminus-driven"), others respond to ice melting at the top surface of the glacier ("runoff-driven"), and still others adjust their water systems as the ice melts, responding to the same melt in a different way ("runoff-adapting"). We do not know the types of all glaciers, nor what causes a glacier to be a certain type.

Previous work identified the types of a few dozen glaciers around Greenland by manually examining ice flow at a single point on each glacier. Here, we take a wider approach by mathematically extracting patterns in ice flow across the entire glacier, not just a single point. We analyze four glaciers that flow into the same fjord in East Greenland. Our results broadly agree with the previous simpler analyses, but differ at two glaciers and identify possible "multi-type" glaciers. Thus, our method holds promise in the quest to discover what controls the seasonal flow patterns of Greenland glaciers.

1 Introduction

Outlet glaciers around Greenland are responding to anthropogenic climate change by retreating, thinning, flowing faster, and increasing their rate of ice discharge into the ocean (Mankoff et al., 2019; King et al., 2020; Mouginot et al., 2019). It is essential that the ice sheet modeling community be able to forecast these changes in aggregate so that stakeholders can plan for sea-level rise and policy makers can enact mitigation measures in the coming decades and centuries. Such forecasts require an understanding of the factors that drive past and ongoing changes in these glaciers so that these factors can be accurately incorporated into ice sheet models. Over the past decade, it has come to light that there is wide variability in the evolution of different Greenland glaciers, both over the multi-year to decadal scale (e.g., Csathó et al., 2014; Bjørk et al., 2018; Mankoff et al., 2019; King et al., 2020; Bevan et al., 2015) and at the sub-annual or seasonal scale (e.g., Moon et al., 2014; Joughin et al., 2019). There is mounting evidence that sub-annual behavior affects the long-term evolution of a glacier: models that resolve a seasonal cycle or include stochastic perturbations produce different results than models that do not (Felikson et al., 2022; Mantelli et al., 2016). Unfortunately, sub-annual patterns of ice flow variability differ from glacier to glacier (Moon et al., 2014; Vijay et al., 2019), and glaciers with similar geometries and climatic forcings, even neighboring glaciers that terminate in the same fjord, often show disparate sub-annual patterns (I. M. Howat et al., 2010, 2010; Vijay et al., 2019; Davison et al., 2020). Overall, we do not yet understand the factors and forcings that change seasonal ice dynamics well enough that these can be accurately represented in ice-sheet models that make sea-level rise predictions.

The advent of accurate, spatially extensive, and temporally dense measurements of ice velocity around the Greenland Ice Sheet (Joughin et al., 2010) facilitated the discovery that different marine-terminating outlet glaciers around Greenland have different seasonal cycles in their flow speed. Pioneering work by Moon et al. (2014) sorted these seasonal flow patterns into three distinct glacier types. Seasonal speed variations of Type 1 glaciers are driven by the position of the terminus. This is because extended terminus positions provide additional sidewall friction that slows ice flow within ∼10 km of the terminus (Moon et al., 2014; I. M. Howat et al., 2010). On Type 2 glaciers, seasonal speed variations are highly correlated to the volume of meltwater runoff in its catchment; annual maximum speeds thus generally occur at the peak of the melt season, in June or July (Moon et al., 2014). Here, the simple conceptual model that basal water reduces friction and speeds ice flow applies. Finally, seasonal speeds on Type 3 glaciers also relate to runoff volumes, but speeds reach their annual maxima in the early melt season, decline by the peak of the melt season, and slowly rise over the autumn, winter, and early spring (Moon et al., 2014). At Type 3 glaciers, the Iken and Bindschadler (1986) or Iken and Bindschadler (1986) model, that the subglacial hydrologic system adapts to accommodate high runoff, applies. For these reasons, Type 1 glaciers are often referred to as "terminus driven", Type 2 as "runoff driven", and Type 3 as "runoff adapting".

Some Greenland glaciers have consistent types, while others can change types from year to year (Moon et al., 2014; Vijay et al., 2019). For instance, a more intense melt season can temporarily drive a normally runoff-driven glacier into runoff-adapting behavior for the year, as was observed by Vijay et al. (2021) during the high melt year 2019. Type can vary not only in time but also in space: neighboring glaciers that terminate into the same fjord can have different seasonal ice flow types, even despite having similar climates, ocean boundary conditions, and basal or sidewall lithologies (Davison et al., 2020).

In Greenland, glacier types have been analyzed island-wide (Moon et al., 2014; Vijay et al., 2019, 2021), within a regional sector (Sakakibara & Sugiyama, 2019), or at focal glaciers (Lemos et al., 2018). These previous studies analyzed ice flow at specific positions along the centerline of each glacier, often located approximately one half-width (a few kilometers) from the terminus, a benchmark set by Moon et al. (2014). Usually, analyses of many glaciers study a single site at each glacier (Moon et al., 2014; Vijay et al., 2019, 2021; Sakakibara & Sugiyama, 2019), while analyses that focus on a smaller number of large glaciers study ice flow at two to eight points along a flowline. For instance, at Zachariae Ice Stream, Lemos et al. (2018) studied three points within 30 km of the terminus, while Ultee et al. (2021) studied 23 points at 1 km spacing on Helheim Glacier, and six points within ∼20 km of the terminus were analyzed at Jakobshavn Glacier by Joughin et al. (2012, 2019), at Helheim and Kangerdlussuaq Glaciers by Kehrl et al. (2017), and at three glaciers feeding Godthabsfjord by Davison et al. (2020). At all these glaciers, the seasonal variations in ice flow were synchronous across all study points, with more muted variability inland that was in phase with the variability nearer the terminus. On Kangerlussuup Sermia, however, the inferred glacier type varied with analysis location. In 2017, this glacier was runoff-adapting within ∼10 km of its terminus, but changed to runoff-driven at distances greater than ∼15 km from its terminus (Vijay et al., 2021). This points to a fundamental limitation of analyses at a small number of points

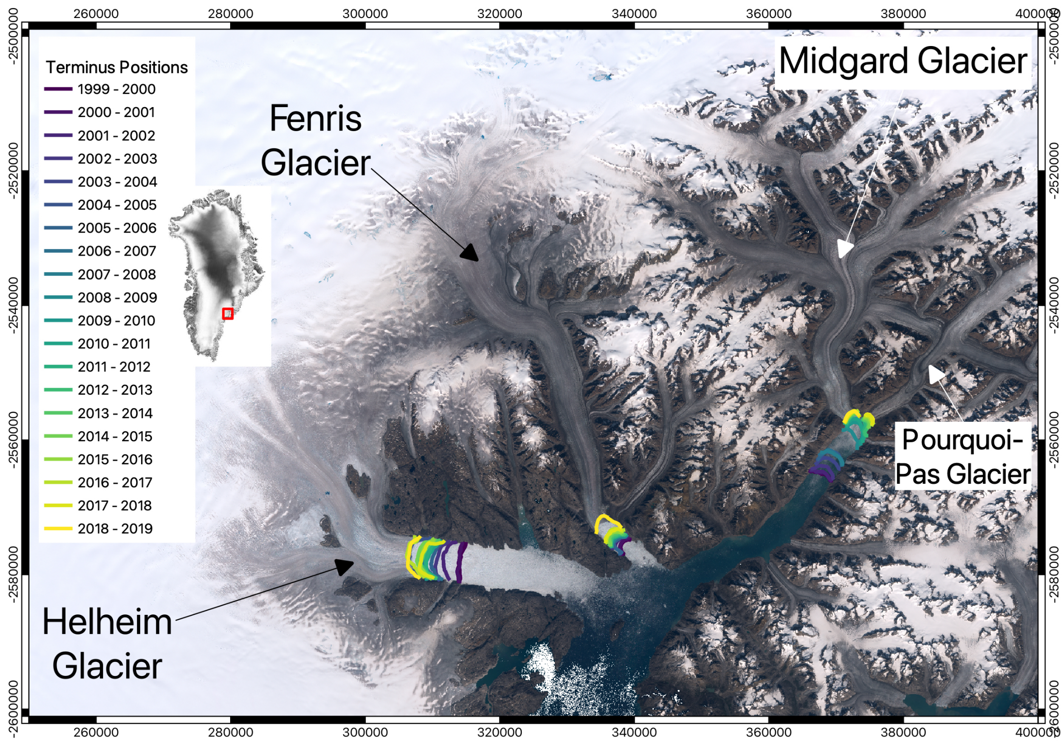

Figure 1. (inset) Location of Sermilik Fjord in eastern Greenland. (main) Sermilik Fjord contains four major outlet glaciers (labeled). The base map is a mosaic of Sentinel-2 images from summer 2019 (MacGregor et al., 2020). The terminus positions from 1999–2019, color-coded by year, are from PROMICE (Korsgaard, 2021).

near the terminus, as has largely been performed on large glaciers to date, and at single points near the terminus, as has commonly been done in ice-sheet-wide studies of glacier type.

Here, we explore the hypothesis that seasonal flow type inferred across an entire glacier trunk may differ from the type inferred from a single point. We focus on four glaciers that terminate in Sermilik Fjord, Southeast Greenland, shown in Figure 1; we use Kangerlussuup Glacier, in central western Greenland, as an additional test case. We use empirical orthogonal function (EOF) / principal component (PC) analysis to extract temporal patterns that are coherent in space across the trunks of four glaciers that terminate in Sermilik Fjord, Southeast Greenland. We infer glacier type from these temporal patterns. Our application of PC/EOF analysis has two advantages: we do not discard information from points off the centerline, and the analysis returns multiple modes of variability, which allows us to infer and quantify the prevalence of multiple glacier types at a single glacier.

To date, the application of EOF / PC analysis within glaciology has been somewhat limited: only Mair (2002); Campbell et al. (2017); Ashmore et al. (2021) have used this technique to interpret glacier flow. Campbell et al. (2017) analyzed the modeled rates of change of ice-surface elevation and speed on Byrd Glacier, Antarctica, over 800-year runs of an ice-flow model. Ashmore et al. (2021) inferred the contributions of terminus position and runoff forcing on a 2.5×4 km area of the main trunk of Jakobshavn Isbrae, approximately 8 km from the terminus. Mair (2002) achieved a similar result on a 0.6×1 km reach of Haut Glacier d'Arolla, Switzerland. Here, we run a similar EOF

Table 1. Velocity datasets used

Glacier	Velocity datasets used	Coverage threshold
Helheim	(A) MEaSUREs Greenland Ice Velocity: Selected Glacier Site Velocity Maps from Optical Images (Howat, 2020) (B) MEaSUREs Greenland Monthly Ice Sheet Velocity Mosaics from SAR and Landsat (Joughin, 2021)	0.85
Fenris	(B) MEaSUREs Greenland Monthly Ice Sheet Velocity Mosaics from SAR and Landsat (Joughin, 2021)	0.5
Midgard	(B) MEaSUREs Greenland Monthly Ice Sheet Velocity Mosaics from SAR and Landsat (Joughin, 2021) (C) MEaSUREs Selected Glacier Site Velocity Maps from InSAR, TerraSAR-X / TanDEM-X (Joughin et al., 2021)	0.95
Pourquoi Pas	(B) MEaSUREs Greenland Monthly Ice Sheet Velocity Mosaics from SAR and Landsat (Joughin, 2021) (C) MEaSUREs Selected Glacier Site Velocity Maps from InSAR, TerraSAR-X / TanDEM-X (Joughin et al., 2021)	0.8
Kangerlussuup	(B) MEaSUREs Greenland Monthly Ice Sheet Velocity Mosaics from SAR and Landsat (Joughin, 2021)	0.95

/ PC analysis of ice speed as Mair (2002); Ashmore et al. (2021), but do so over full-glacier analysis domains sized 150–350 km^2.

2 Methods

2.1 Datasets Used

2.1.1 Glacier velocity data

We use velocity data from three different sources, listed in Table 1 and plotted in Figure 2. These datasets are a 100-m resolution velocity product derived from Landsat-8 and ASTER images created through the Greenland Ice Sheet Mapping Program (GrIMP) within the NASA MEaSUREs program (Howat, 2020); a 200-m resolution ice-sheet-wide monthly-average velocity product generated from SAR and Landsat images (Joughin, 2021; Joughin et al., 2010, 2018), and a 100-m resolution product generated for specific glaciers from InSAR from image pairs acquired by the TerraSAR-X and TanDEM-X satellites (Joughin et al., 2021, 2010). The spatial resolution of these datasets vary from 100 to 200 meters; we interpolate all observations onto a common 600 $\times$ 600 m grid specific to each glacier. We discard directional (velocity) information, retaining only speed. The temporal spacing varies in time and is driven jointly by the interval of the velocity product (8–30 days) and our selection of scenes based on the completeness of spatial coverage. Across all glaciers we analyzed, the average temporal spacing was 34 days.

The quality and availability of each dataset varies glacier by glacier. We experimented with using different combinations of available datasets across each glacier. We ultimately selected datasets that had good coverage over 2016–2021, had a low error-to-magnitude flow speed ratio, and gave coherent EOF / PC results. The velocity datasets used in the analyses are listed in Table 1. We also required each scene to have a minimum threshold of coverage over our study area; this threshold varies by glacier, from

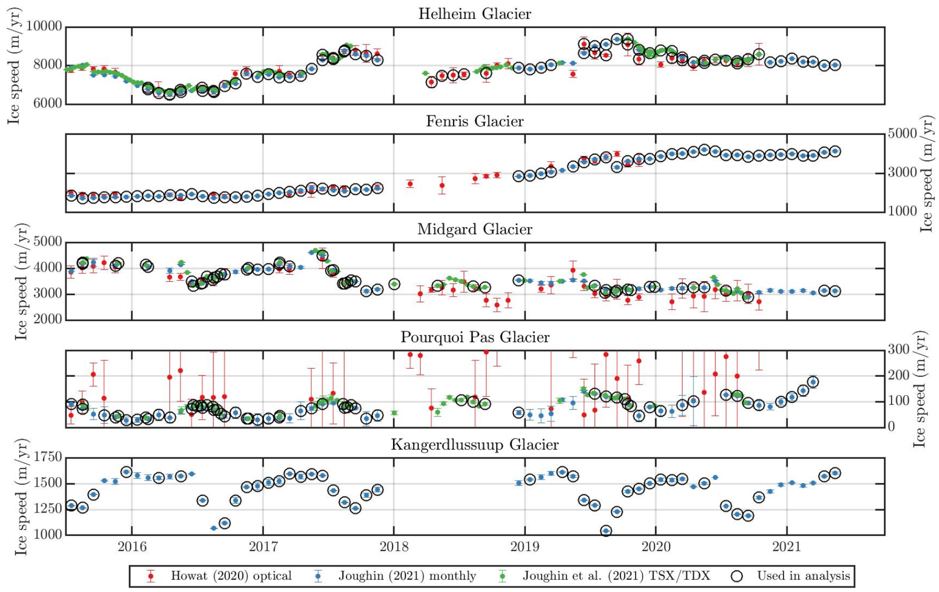

Figure 2. Velocity datasets used in this analysis (Howat, 2020; Joughin, 2021; Joughin et al., 2021). Speeds at specific points near the terminus of each glacier (green stars on Figures 5–8) are shown in color, with error bars. For each glacier, we used specific scenes, which are circled in black.

50% to 95%, as shown in Table 1. Scenes that meet this criterion are circled in black in Figure 2.

2.1.2 Runoff data

We use runoff data from MERRA-2 (Rienecker et al., 2011) over 2015–2021. We extract these data at the point on each glacier analyzed by Vijay et al. (2019). The MERRA-2 data have 1-hour resolution; we smooth them over 14 days using a pseudo-Gaussian filter.

2.1.3 Terminus position data

Where available, we use pre-existing terminus position datasets for each glacier. For Helheim Glacier, we use the TermPicks dataset (Goliber et al., 2022), which averages 3-day resolution and extends through June 2020. For Midgard and Pourquoi Pas Glaciers, the resolution and extent of TermPicks are insufficient (140-day resolution through March 2019); this was also true of Fenris Glacier (40-day resolution through June 2019). Therefore, for these three glaciers, we generated our own terminus position dataset using the Google Earth Engine Digitisation Tool (GEEDiT) software (Lea, 2018). We digitized the terminus position along the glacier centerline when it was visible in all available Landsat 8 and Sentinel 2 images acquired over 2015–2021 with ¡50% scene cloud coverage. These three new terminus datasets each average 6-day resolution and extend through October 2021. For Kangerdlussuup Glacier, we also use TermPicks (Goliber et al., 2022), which averages 19-day resolution and extends through February 2020.

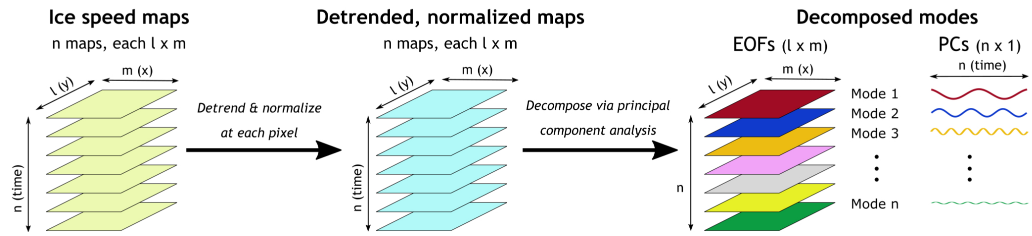

Figure 3. Schematic of the EOF/PC analysis process. We begin with a stack of n maps of ice speed for a given glacier, all with the same footprint ($l \times m$ pixels in x-y space; yellow at left). At each pixel, we remove any trend in the $1 \times n$ timeseries, then normalize it (cyan at center). Finally, we use MATLAB's `pca` function to decompose the map-based timeseries into n modes, shown in bold colors at right, each with an empirical orthogonal function (EOF) that shows the spatial patterns (sized $l \times m$) and a principal component (PC) that gives the mode's corresponding pattern in time (sized $n \times 1$). The modes are sorted from largest (mode 1) to smallest (mode n) amount of variance explained in the normalized, detrended dataset.

2.2 EOF/PC Decomposition

Empirical orthogonal function (EOF) / principal component (PC) analysis reduces a dataset of many variables – in our case, observations of ice flow speed at thousands of points – into one of only a handful of variables that capture the essence of the original data (Lorenz, 1956; Wilks, 2019). These new variables, or modes of variability, are linear combinations of the original variables and are orthogonal to all other modes. Each mode has a spatial component (EOF) that pairs one-to-one with its temporal variability (PC), and the modes are sorted according to the amount of variance they explain. The leading modes (highest variance explained) often, but are not mathematically required to, represent a distinct phenomenon that gives rise to a unique spatio-temporal pattern. For example, the Arctic Oscillation is the first mode of the wintertime sea-level pressure field in the northern hemisphere (Lorenz, 1951; Thompson & Wallace, 1998), and the first mode of ice flow speed in a specific area of Jakobshavn Isbræ captures the effects of seasonal stress changes at the glacier terminus (Ashmore et al., 2021).

EOF/PC analysis is useful for datasets where each observation has a high degree of correlation to other observations. This includes many map-based datasets, including sea-level pressure (e.g., Lorenz, 1956; Smoliak & Wallace, 2015), rainfall (e.g., Mishra et al., 2012), and a plethora of other meteorological and geophysical variables. In our case of ice flow speed, each observation within a pixel sized <1 km^2 indeed varies little from the value in the next pixel.

As described in Section 2.1.1, we use multiple velocity datasets for each glacier, but we select only scenes that exceed a minimum threshold of coverage (Table 1). Next, we detrend the observations at each pixel using an ordinary least squares fit, then normalize each observation by the mean speed at that pixel over the observation interval. Then, we perform EOF / PC analysis using the MATLAB function `pca` and the alternating least squares algorithm, option `'als'`, to fill pixels that lack observations. We restore the mean velocity magnitudes to the EOFs (spatial patterns) by multiplying each pixel (loading) by its mean speed over time. Finally, we scale each PC (temporal pattern) so that its maximum value (score) is 1, then apply the inverse of this scale to all loadings in the corresponding EOF. We run the analysis over each glacier separately. Figure 3 shows our workflow.

For a stack of n scenes, where n is the length of our time series, with each scene sized $l \times m$ pixels in x-y space, EOF / PC analysis returns n modes of variability. Each mode comprises an EOF, which is sized $l \times m$ in x-y space and gives the spatial pattern of variability; a PC, which is sized $n \times 1$ and shows the strength of the corresponding spatial pattern over time; and an eigenvalue, which gives the amount of variance in the dataset explained by that mode. Each point in the PC corresponds directly to the timestamp of each velocity scene. In our case, the length of the time series n is much shorter than the number of pixels in each scene (for example, on Helheim Glacier, $n = 72$, $l = 351$, $m = 281$, and $l \times m = 98{,}631$), which limits the number of modes returned to n. In other cases with very long time series or small spatial footprints ($n > l \times m$), EOF / PC analysis would return more modes ($l \times m$).

All modes are orthogonal to all other modes. This makes EOF / PC analysis well suited to the glacier type problem, since the forcings are also largely orthogonal: time variations in terminus position, for instance, are never directly obtainable from time variations in runoff volumes or the capacity of the subglacial hydrologic system. Thus, different modes of glacier speed should correlate to these different forcings. One mode may significantly correlate to more than one forcing, and one forcing may correlate to more than one mode, but the degree of correlation will differ.

Although most velocity datasets we used come with measurement errors, we do not incorporate these values into our analysis. Penalizing errors, which in our case are often largest at the same locations over time, tends to return single modes that contain very high amounts of the variance. In our case, we found leading modes that explained >99% of the variance when we penalized observations by the raw error value, and similar results when we penalized by the error value normalized by the mean local speed. This result is less useful because it returns one dominant pattern that magnifies the contribution of the many points far upglacier, minimizes that of the fewer points near the terminus, and fails to separate any distinct patterns of variability that may be present in space and/or time. On the marine-terminating glaciers we analyze, the most significant annual variations in speed occur near the terminus; an ideal analysis will incorporate these variations at least as prominently, if not more prominently, than data at upglacier locations that are more steady in time. Overall, since measurement errors tend to be largest near the terminus, we did not use measurement errors in our EOF / PCA analysis. We did consider the magnitude of the errors when selecting which datasets to use for each glacier (Section 2.1.1 and Figure 2).

2.3 Identification of Seasonal Cycles in PCs

We fit a curve with four free parameters to each PC time series:

$$PC = a_0 + a_1 t + a_2 \left(\frac{2\pi t}{T} \right) + a_3 \left(\frac{2\pi t}{T} \right) \tag{1}$$

Here, the principal component value is PC, time (in days) is t, and the annual period (365.25 days) is T. An ordinary least-squares regression returns coefficients a_0, a_1, a_2, and a_3. Because we detrend each time series before performing EOF/PC analysis, a_1 is always zero. From a_2 and a_3, we derive the timing of the mean annual maximum and minimum glacier speed for each mode and for each time interval. We perform a one-sided t-test for significance of correlation between each PC and the fitted annual cycle y:

$$y = a_2 \left(\frac{2t}{T} \right) + a_3 \left(\frac{2t}{T} \right) \tag{2}$$

$$t = \frac{r\sqrt{n-2}}{\sqrt{1-r^2}} \tag{3}$$

where r is the correlation coefficient between the PC and the annual cycle y, each of which has n observations in time. Finally, we calculate the p value using the Student's t cumulative distribution function in Matlab, `tcdf`, and interpret it as significant when $p < 0.05$.

2.4 Correlation analysis of PCs and terminus position

For all glaciers, we detrend the terminus position dataset within the analysis period, then linearly interpolate the terminus position onto the observation dates of the PC, and finally calculate the correlation coefficient and performed a one-sided t-test for significance of correlation between each PC and the terminus position, as above. Note that a negative correlation is expected between terminus position, which is longer when the glacier front extends farther into the fjord, and glacier speed, which should decrease with a longer glacier that exerts more sidewall buttressing onto the ice. Thus, we accept significance only when the correlation coefficient is negative.

2.5 Identification of glacier type

We classify glaciers whose leading PCs had significant anti-correlation to terminus position as terminus-driven. For runoff-driven glaciers, we require significant correlation between the PC and a seasonal cycle with peak speed occurring during the peak melt season, which we define as June through August. For runoff-adapting glaciers, we require significant correlation with peak speed before peak melt, which we define as March through May. If any glacier lacks significant ($p < 0.05$) correlation across all three possibilities, we leave it unclassified.

3 Results

For all glaciers we studied, we find that the leading-order mode for all glaciers has uniformly signed variability over the entire domain, and that this mode explains the majority of the variance in ice flow speed. This amount ranged from 70% of the variance (Fenris and Pourquoi Pas Glaciers) to 95% of the variance (Helheim Glacier). At all glaciers, the first EOF was uniformly signed across all or nearly all of the domain, indicating that the majority (70–95%) of the seasonal and inter-annual variance of ice flow at any point occurs in sync with other points. The only exception to this observation was at two glaciers with significant calving front retreat over the analysis period. At these glaciers (Midgard and Pourquoi Pas), the first EOF had the opposite sign in the small area of calving front variability than in the rest of the domain.

EOF/PC analysis forces random or otherwise non-coherent variability into higher-order modes. This variability can be due to random errors, grid artifacts, or other specific circumstances that interfere with image correlation, such as cloudiness or water at the surface (Poinar & Andrews, 2021). We found such features in modes 3 and higher (Midgard and Fenris Glaciers), mode 5 and higher (Helheim Glacier) or mode 8 and higher (Pourquoi Pas Glacier). On Midgard and Fenris Glaciers, this accounted for 7–10% of the variance, while on Helheim and Pourquoi Pas Glaciers, it accounted for <1% of the variance.

The results of our classification and their comparison to previous work are summarized in Table 2.

Table 2. Summary of glacier type classification. References are M for Moon et al. (2014), V1 for Vijay et al. (2019), and V2 for Vijay et al. (2021). The variable c denotes correlation coefficient, N denotes the number of velocity scenes, p denotes p-value, and ✓ and × symbols denote significance or lack of significance, respectively.

	Helheim Glacier	Fenris Glacier	Midgard Glacier	Pourquoi-Pas Glacier
Previous classification	Terminus-driven in 2009–2010 and 2015–2017 (M, V1) Runoff-driven in 2013 and 2009 (M)	Terminus-driven in 2015–2017 (V1)	Runoff-adapting in 2011–2019 (M, V1, V2)	Terminus-driven in 2015–2017 (V1)
This work's classification (2016–2021)	Primarily terminus-driven ($p < 10^{-4}$) Secondarily runoff-driven ($p < 10^{-3}$)	Runoff-adapting ($p = 0.002$)	Runoff-adapting ($p < 10^{-6}$)	Runoff-driven ($p < 10^{-8}$)
Agreement?	✓	×	✓	×
Correlation of PC with single point	$c = 0.58, N = 72$ $p < 10^{-7}$ ✓	$c = 0.05, N = 58$ $p = 0.3$ ×	$c = 0.55, N = 56$ $p < 10^{-5}$ ✓	$c = 0.69, N = 64$ $p < 10^{-9}$ ✓

3.1 Helheim Glacier

3.1.1 Leading mode (95%): terminus-driven and runoff-driven

Figure 4 shows the first two modes of the decomposition of ice speed on Helheim Glacier. The first mode explains 95% of the variance in ice flow that occurred at 72 image pair midpoints (observation times) between February 2016 and May 2021. The first EOF (Figure 4a) reaches up to 9 km/yr on the lower main trunk of the glacier and decays to <1 km/yr in the margins and upper reaches of the domain. On the southern branch of the glacier, the EOF reaches a maximum of 4 km/yr. The first mode encompasses both the time-mean flow speed at each point (the EOF) and its variability (the PC).

Figure 4c shows the first PC, which ranges from a minimum of 0.82 to a maximum of 1. Thus, the minimum detrended ice flow speed observed at any location is 0.82 times the value of the EOF (loading) there, within 5% (since the first mode explains 95% of the variance); and similarly for the maximum. In the center of the lower glacier (green star on Figure 4a), these inferred minimum and maximum speeds are respectively 7.0 km/yr and 8.5 km/yr. These compare well to the detrended observations at this point, with minimum 6.8 km/yr (within 3% of the first-mode-only value) and maximum 8.9 km/yr (within 5%).

We infer glacier type from the leading-order PC (Figure 4c). This PC significantly anti-correlates with the detrended TermPicks terminus position (magenta; $p < 10^{-4}$) and significantly correlates with the MERRA-2 runoff on the lower glacier (black; $p < 10^{-3}$), both shown in Figure 4e. It also significantly correlates with a fitted annual cycle that reaches a maximum speed in mid-August ($p = 0.005$), shown in Figure 4c (dashed line). Because the correlation between the PC and the terminus position is strongest, we infer primarily Type 1 (terminus-driven) behavior for Helheim Glacier. We infer sec-

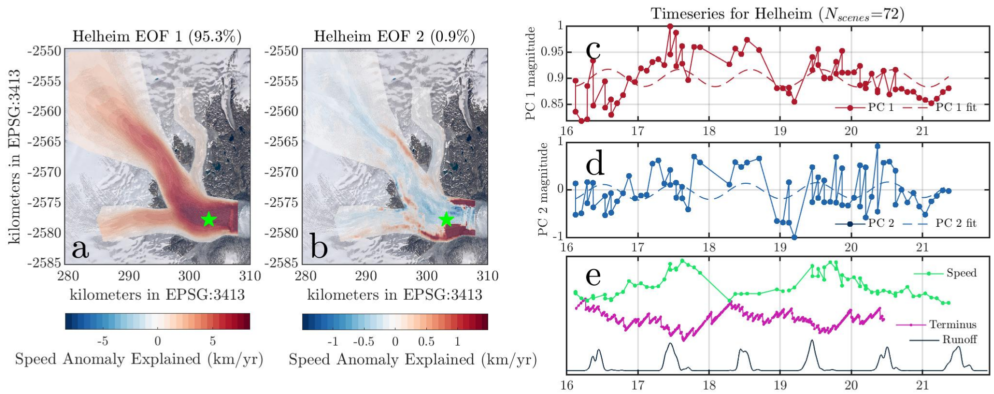

Figure 4. EOF/PC decomposition for the detrended speed of Helheim Glacier for observations at 72 times over the period 2016–2021. (a) First EOF, which pairs with the first PC to explain 95% of the variance in the entire dataset. Green star shows the location of the speed data plotted in panel e. (b) Second EOF, which pairs with the second PC to explain 1% of the variance in speed. (c) First PC (points with spline fit) and a fitted annual cycle (dotted line) that peaks in mid August. (d) Second PC (points with spline fit) and a fitted annual cycle (dotted line) that peaks in mid July. (e) Detrended timeseries of speed at the locations of the green star (green), detrended terminus position (pink) from TermPicks (Goliber et al., 2022), and runoff at the green star from MERRA-2 (black) (Rienecker et al., 2011).

ondary runoff control because of the next-highest correlation with runoff and a seasonal cycle that peaks during summer.

The first PC correlates significantly ($p < 10^{-7}$) with the detrended flow speed at a point on the lower glacier studied by Vijay et al. (2019), shown in green in Figure 4e. From this agreement, we conclude that ice flow on Helheim can reliably be classified by analyzing data at that single point, as previous analyses have done. However, our EOF/PC analysis yields further insight: the terminus position correlates more highly with the speed at the single point ($p < 10^{-15}$) than it does with the first PC ($p < 10^{-4}$, as stated above), while the runoff timeseries correlates more highly with the first PC ($p < 10^{-3}$, also above) than with the single-point time series ($p = 0.02$). This implies that runoff drives ice flow variability over the entire glacier, rather than just at a single point, whereas the influence of the terminus is more limited to points near the terminus.

3.1.2 Second mode (1%): Runoff-driven with spatial differences

The second mode explains 1% of the variance in flow speed over 2016–2021. The second EOF (Figure 4b) separates the glacier margins, especially those in the lowermost 10 km (dark red), from the rest of the analysis domain. The southern margin so defined is wider (∼2 km) than the northern margin (∼1 km). Up to 8 km/yr of ice flow variability occurs in the second mode; these dynamic areas are positively signed (red) and are within 2 km of the terminus, which roughly encompasses the range of terminus variability over this time period (Goliber et al., 2022; Cheng et al., 2021). Farther upglacier, the margins remain positively signed but contain less variability – e.g., 200–500 m/yr fifteen kilometers from the terminus. Along the centerline of the glacier, however, the first EOF represents <1 km/yr of variability and is negative (blue), indicating that in this mode, the centerline and margins have opposing variability.

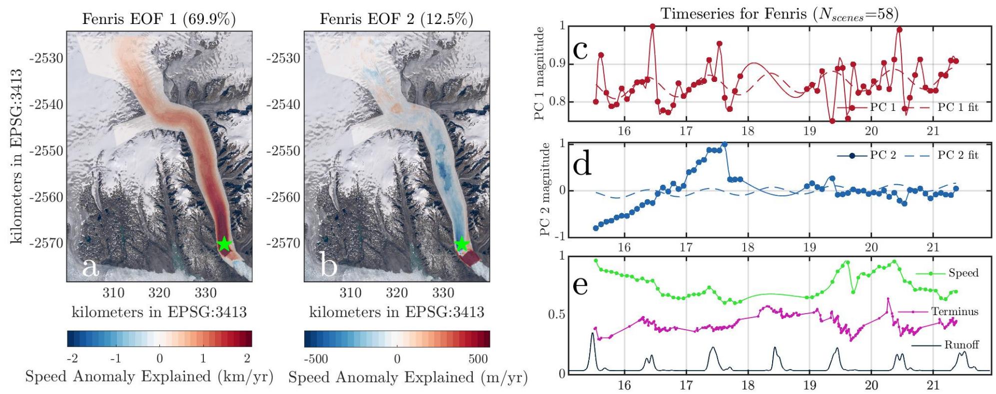

Figure 5. EOF/PC decomposition for the detrended speed of Fenris Glacier for observations at 58 times over the period 2015–2021. (a) First EOF, which pairs with the first PC to explain 70% of the variance in the entire dataset. Green star shows the location of the speed data plotted in panel e. (b) Second EOF, which pairs with the second PC to explain 13% of the variance in speed. (c) First PC (points with spline fit) and a fitted annual cycle (dotted line) that peaks in mid May. (d) Second PC (points with spline fit) and a fitted annual cycle (dotted line) that peaks in mid May. (e) Detrended timeseries of speed at the locations of the green star (green), detrended terminus position (pink) identified using GEEDiT (Lea, 2018), and runoff at the green star from MERRA-2 (black) (Rienecker et al., 2011).

The second PC (Figure 4d), like the first PC, significantly correlates with the runoff time series ($p = 0.01$) and has a significant annual cycle ($p = 0.008$) that peaks in mid-July; this is consistent with a runoff-driven glacier. The second PC does not correlate significantly with terminus position ($p = 0.1$) or with ice flow at the Vijay et al. (2019) green star location ($p = 0.2$). The similar phasing to the first PC, which peaks in mid-August, suggests that the second mode primarily modifies the spatial pattern of the first mode: the true seasonal cycle in speed along the centerline is well represented by the first mode, but in the margins, and especially in the margins within 10 km of the terminus, the the seasonal cycle is a few hundred meters per year lower in magnitude than shown by the first mode alone, and lags the first PC by about one month.

3.2 Fenris Glacier

3.2.1 Leading mode (70%): Runoff-adapting

Figure 5a shows the first EOF for Fenris Glacier from October 2015 through May 2021. The first mode explains 70% of the variance in ice flow over this period. The EOF is highest-magnitude in the glacier trunk, where it explains >2 km/yr. Near the Vijay et al. (2019) point 5 km inland from the terminus (green star), the magnitude of the first EOF is 3.3 km/yr, which is comparable to the local mean annual flow speed, ∼5 km/yr, and its interannual variability, ∼3 km/year. The magnitude of the EOF decays in the margins, in the upper tributaries (>40 km from the terminus), and in the area immediately (<5 km) adjacent to the terminus, which was ice-covered until it experienced rapid retreat beginning in 2018 (Korsgaard, 2021).

The first PC (Figure 5c) significantly correlates with an annual cycle with a maximum speed in mid-May ($p = 0.0004$). It does not significantly correlate with terminus position ($p = 0.4$, Figure 5e), but it does with the runoff record ($p = 0.02$), albeit less well than with the early-season cycle. These findings are consistent with Fenris Glacier behaving as a runoff-adapting glacier over 2016–2021.

The first PC does not significantly correlate with the speed at the point studied by Vijay et al. (2019), shown in green in Figure 5e ($p = 0.3$). This indicates that the first mode includes significant variability at places other than the near-terminus area. Fenris Glacier is the only glacier in our study whose first PC did not significantly correlate to the speed at the Vijay et al. (2019) analysis point.

3.2.2 Second mode (13%): Interannual variability and terminus–trunk differences

The second mode contains 13% of the variance in the flow of Fenris Glacier. Figure 5b shows this EOF, which contains a near-terminus dipole – the high-magnitude (∼2 km/yr), positively-signed southernmost 2 km of the glacier and the lower-magnitude (<500 m/yr) negatively signed areas in the trunk ∼2–20 km from the terminus. The dipole coincides with the location of terminus retreat over 2018–2019 (Figure 5d). At the terminus, the magnitude of the second EOF reaches its maximum of 2 km/yr; at the Vijay et al. (2019) analysis point 5 km inland from the terminus (green star), the magnitude is -400 m/yr. Especially at the terminus, this is a significant fraction of the mean annual flow speed (∼5 km/year) and its annual and interannual variability (∼3 km/year).

The second PC (Figure 5c) shows a steady change over 2016–2017, then near-zero magnitude over 2019–2021. Recall that we detrended the speeds at each pixel before performing EOF/PC analysis; thus, the analysis is blind to the 2016–2020 speedup of the glacier. Thus, the 2016–2017 trend in the PC reflects an additional speedup of the main trunk (2–20 km upstream of the terminus) totaling up to 800 m/yr over that period, alongside a substantial ∼4 km/yr slowdown near the terminus, beyond what is captured by the first mode alone. Said another way, the first mode overestimates the speedup near the terminus over 2016–2017, and the second mode corrects for that. The near-zero values over 2019–2021, on the other hand, show that the first mode explains much of the variance over that period.

Over the full interval 2015–2021, the second PC shows no significant annual cycle ($p = 0.06$), correlation with runoff volumes ($p = 0.1$), or terminus position ($p = 0.2$). The second PC correlates significantly with ice flow at the Vijay et al. (2019) point ($p < 10^{-6}$); recall that the first PC did not.

3.3 Midgard (Franche Comté) Glacier

This glacier, located at 66.48°N, 36.72°W, takes various names: most commonly Midgard Glacier (Moon et al., 2014; Mouginot et al., 2019), but also Franche Comté Glacier (Bjørk et al., 2015; Goliber et al., 2022; Vijay et al., 2019) or Midgard North (Walsh et al., 2012; Williams, n.d.). This glacier extended 10 km farther down its fjord as recently as 2002, but since has retreated rapidly and split into two glaciers around 2012. We use the name Midgard Glacier to refer to the larger, more northwestern of the two termini that share this fjord.

3.3.1 Leading mode (85%): Runoff-adapting

Figure 6a shows the first EOF for Midgard Glacier over October 2015 through May 2021. The first mode explains 85% of the variance in ice flow over this period. The EOF is highest-magnitude in the glacier trunk within ∼3 km of the terminus, where it reaches 7 km/yr. For comparison, the local mean annual flow speed there ranges from ∼4–7 km/year and has variability of 0.5–1 km/year over our study interval. The magnitude of the EOF decays upstream, toward the margins, and in the five tributaries. This EOF is positive

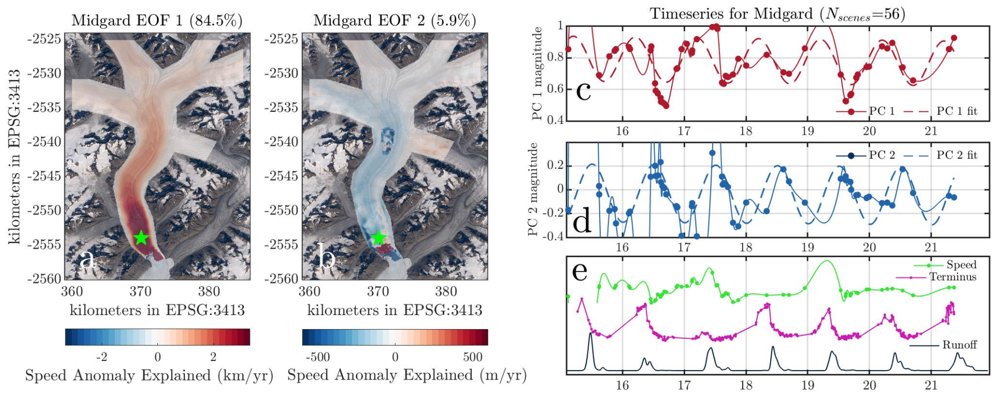

Figure 6. EOF/PC decomposition for the detrended speed of Midgard Glacier for observations at 56 times over the period 2015–2021. (a) First EOF, which pairs with the first PC to explain 85% of the variance in the entire dataset. Green star shows the location of the speed data plotted in panel e. (b) Second EOF, which pairs with the second PC to explain 6% of the variance in speed. (c) First PC (points with spline fit) and a fitted annual cycle (dotted line) that peaks on in mid March. (d) Second PC (points with spline fit) and a fitted annual cycle (dotted line) that peaks in mid July. (e) Detrended timeseries of speed at the locations of the green star (green), detrended terminus position (pink) identified using GEEDiT ((Lea, 2018), and runoff at the green star from MERRA-2 (black) (Rienecker et al., 2011).

everywhere except the immediate terminus area, where the calving front has fluctuated over the analysis period.

The first PC (Figure 6c) significantly correlates with an annual cycle with a maximum speed in mid March ($p < 10^{-9}$) and with the runoff record ($p < 10^{-3}$). The first PC correlates positively with terminus position; recall that a negative correlation is expected if terminus position drove the flow speed. From these results, we conclude that Midgard Glacier was runoff-adapting over 2016–2021.

The first PC significantly correlates with the speed at the point studied by Vijay et al. (2019), shown in green in Figure 6e ($p < 10^{-5}$), suggesting that classifications using that point alone are reliable.

3.3.2 Second mode (6%): Runoff-driven

The second mode contains 6% of the variance in the flow of Midgard Glacier. Its EOF, shown in Figure 6b, consists of a dipole that separates the near-terminus area (¿2 km/yr) from the main trunk of the glacier (<400 m/yr). The inflection point of the dipole stands ∼2 km inland of the farthest retreat point of the calving front, suggesting that this is a real zone of terminal influence, rather than an artifact of calving front retreat over the study period, as on Fenris Glacier. The second EOF also separates the four northern and eastern tributaries (positively signed) from the main trunk and the westernmost tributary (negatively signed). Finally, the easternmost tributary of the glacier appears more strongly in the second EOF (160 m/yr) than in the first EOF (<50 m/yr), suggesting that the second mode best represents glacier flow here.

The second PC (Figure 6d) shows a strong seasonal cycle with a peak in mid July ($p < 10^{-8}$). It significantly correlates to the runoff time series ($p < 10^{-4}$) but not to the terminus position ($p = 0.07$). The second PC is not significantly related to ice flow

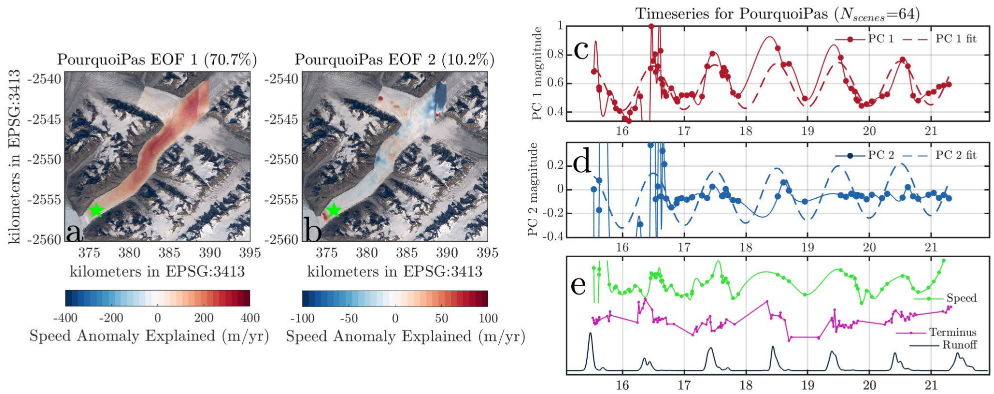

Figure 7. EOF/PC decomposition for the detrended speed of Pourquoi Pas Glacier for observations at 64 times over the period 2015–2021. (a) First EOF, which pairs with the first PC to explain 71% of the variance in the entire dataset. Green star shows the location of the speed data plotted in panel e. (b) Second EOF, which pairs with the second PC to explain 10% of the variance in speed. (c) First PC (points with spline fit) and a fitted annual cycle (dotted line) that peaks in mid July. (d) Second PC (points with spline fit) and a fitted annual cycle (dotted line) that peaks in mid July. (e) Detrended timeseries of speed at the locations of the green star (green), detrended terminus position (pink) identified using GEEDiT (Lea, 2018), and runoff at the green star from MERRA-2 (black) (Rienecker et al., 2011).

at the Vijay et al. (2019) location ($p = 0.3$). This suggests that in the immediate terminus area, runoff control is a highly secondary influence on ice flow (6% of the variance), while in the easternmost tributary it is a primary influence.

3.4 Pourquoi-Pas (East Midgard) Glacier

This glacier, located at 66.46°N, 36.65°W, separated from Midgard Glacier in 2012 (Korsgaard, 2021). It is significantly smaller and less well studied than the other glaciers in the fjord, and many databases omit its name (Bjørk et al., 2015; Mouginot et al., 2019) or refer to it as Midgard South (Williams, n.d.) or Midgard Glacier (Goliber et al., 2022; Vijay et al., 2019; Walsh et al., 2012), as it lies directly upfjord of the reach that Midgard used to occupy before its split. The northwestern tributary is significantly larger and we term it Midgard Glacier (Section 3.3). For this eastern tributary, we adopt the name for its upstream branch used thirty years ago by an English mountaineering expedition: Pourquoi Pas Glacier (Gregson, 1995).

Upon separating from Midgard Glacier, the immediate terminus area of Pourquoi Pas Glacier slowed significantly, to less than half its previous speed. The terminus area retained a seasonal cycle with the same phasing as before, but lower magnitude.

3.4.1 Leading mode (71%): Runoff-driven

Pourquoi Pas Glacier is unusual in that its fastest-moving ice is upstream, ∼20 km from the terminus, where the speed reaches 200 m/yr. A second local rapid area sits ∼10 km from the terminus, where the ice moves 140 m/yr. Ice within 1 km of the terminus moves only ∼80 m/yr. Each of these local maxima are separated by slower-moving ice, as low as 60 m/yr. The first EOF over October 2015 through May 2021 (Figure 7a) captures the upstream-most and the mid-trunk maxima, but not the maximum near the terminus.

The first mode explains 71% of the variance in ice flow over this period. The EOF (Figure 7a) is positive everywhere except within a few hundred meters of the terminus. It is highest-magnitude 10–15 km upstream of the terminus, where it explains 300 m/yr, which is greater than the local mean annual flow speed ($\sim$200 m/yr). Near the Vijay et al. (2019) analysis point $\sim$1 km inland from the terminus, the magnitude of the first EOF is 130 m/yr, also greater than the local mean annual flow speed, 70 m/yr. This implies a significant contribution from higher-order modes near the terminus.

The leading PC (Figure 7c) significantly correlates with an annual cycle peaking in mid-July ($p < 10^{-12}$) and with the runoff record ($p < 10^{-5}$), both shown in Figure 7e. It does not significantly correlate to terminus position ($p = 0.3$). This implies that Pourquoi Pas Glacier was runoff-driven over 2016–2021. This PC significantly correlates with the speed at the point studied by Vijay et al. (2019), shown in green in Figure 7e ($p < 10^{-9}$), indicating that a single-point analysis would be sufficient for classifying this glacier.

3.4.2 Second mode (10%): Interannual variability

Like the first PC, the second PC (Figure 7d) also implies runoff-driven behavior. It correlates significantly with an annual cycle peaking in mid-July ($p < 10^{-6}$) and with the runoff record (p=0.04), but not with terminus position ($p = 0.4$). The mid-summer phasing of the annual cycle fit is nearly identical to that of PC 1. However, PC 2 has periods of relative quiescence (2017, 2019–2021) interspersed with years with strong seasonal cycles (2015–2016, 2018). This suggests that the second mode tends to intensify (where the EOF is positive) or mute (where it is negative) the seasonal patterns of the first mode, but that this occurs intermittently from year to year.

Pourquoi Pas Glacier has a section on its main trunk, between 2–10 km from its terminus, that slows substantially over September through April, then reactivates each spring. Thus, the seasonal cycle in this reach is stronger than that of the ice around it. This appears in the second EOF as a relatively uniform stretch of approximately -30 m/yr across this reach. The second PC adds (winter) or subtracts (summer) this 30 m/yr from the speed of the first mode, with which it is antiphased. The second EOF is also high-magnitude in the uppermost reaches of the glacier, where it is negatively signed and thus adds (winter) or subtracts (summer) up to 1 km/yr from the first mode. Near the terminus, the second EOF is positive at 100 m/yr, and adds in phase with the first mode. Note that the second PC shows that these patterns apply primarily in 2015–2016 and 2018, while in other years, the influence of the second mode is negligible.

3.5 Comparison to Analysis at a Single Point

Significant correlation between a PC and a detrended single-point speed indicates that our classification of glacier type should agree with that done by analyzing the single point, i.e. the classifications of Moon et al. (2014). A lack of significant correlation implies that flow over the entire glacier is more complex than what is observable at a single point, and in these cases we might expect our classifications to differ.

As described in the above sections, we found significant correlation between the first PC and the detrended ice flow speed at the near-terminus points for Helheim, Midgard, and Pourquoi-Pas Glaciers, but not at Fenris Glacier. Separately, our classification of Helheim as terminus-driven and Midgard as runoff-adapting agrees with previous analyses (Moon et al., 2014; Vijay et al., 2019, 2021), while our classification of Fenris as runoff-adapting over 2016–2021 disagrees with its previous classification as terminus-driven over 2015–2017 (Vijay et al., 2019). Finally, our assessment of Pourquoi-Pas Glacier as runoff-

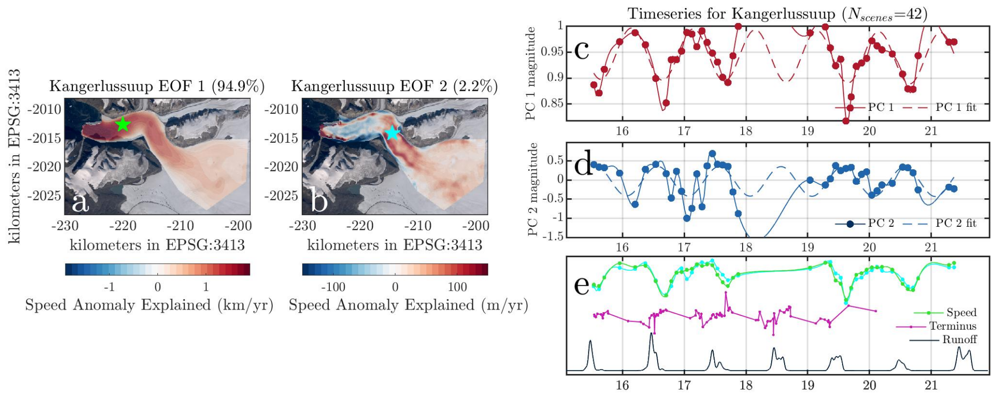

Figure 8. EOF/PC decomposition for the detrended speed of Kangerdlussuup Glacier, western Greenland, for observations at 42 times over the period 2014–2021. (a) First EOF, which pairs with the first PC to explain 95% of the variance in the entire dataset. Green star shows the location of the speed data plotted in panel e. (b) Second EOF, which pairs with the second PC to explain 2% of the variance in speed. (c) First PC (points with spline fit) and a fitted annual cycle (dotted line) that peaks in mid February. (d) Second PC (points with spline fit) and a fitted annual cycle (dotted line) that peaks in mid July. (e) Detrended timeseries of speed at the locations of the green and cyan stars (colored respectively), detrended terminus position (pink) from TermPicks (Goliber et al., 2022), and runoff at the green star from MERRA-2 (black) (Rienecker et al., 2011).

driven over 2016–2021 is also at odds with the classification of terminus-driven in 2015–2017 by Vijay et al. (2019).

A fundamental difference in technique likely explains these discrepancies. Our analysis parallels that of Moon et al. (2014) in that we first detrend the speed at each pixel before analyzing the seasonal patterns. Vijay et al. (2019, 2021), however, left trends intact. Comparison of the Moon et al. (2014) and Vijay et al. (2019) analyses shows that they agree on the type of 60% (7 of 11) of glaciers and disagree on 40% (4 of 11). Vijay et al. (2019) classified Fenris and Pourquoi Pas Glaciers based on their long-term trends of increasing ice speed, which was coincident with the retreat of their termini. This likely accounts for the difference with our classification, which is based solely on seasonal cycles.

3.5.1 Test at Kangerlussuup Sermia, western Greenland

Vijay et al. (2021) identified Kangerlussuup Sermia (71.45°N, 51.36°W) as having variable type along flow: it was runoff-adapting near its terminus, but changed to runoff-driven near a bend ∼12 km from its terminus. We test our method's ability to detect this spatial change in type by performing our analysis on Kangerlussuup Sermia, which is located in western Greenland ∼30 km south of Rink Glacier. Figure 8 shows our results over 2016–2021. Near the terminus, the first mode accounts for almost 2 km/year of ice flow; by ∼15 km from the terminus, it drops to ∼1 km/year and continues to decline inland (Figure 8a). The first PC (Figure 8c) correlates significantly with an annual cycle with peak speed in March ($p < 10^{-8}$), but not with terminus position ($p = 0.2$) or runoff data itself ($p = 0.4$). This is consistent with a runoff-adapting glacier. This runoff-adapting mode explains 95% of the variance in speed.

Figure 8b shows the second EOF at Kangerlussuup Sermia over 2016–2021. It is a dipole with a hinge point at the bend ~12 km from the terminus. Upstream of the hinge and in the glacier margins, the EOF is positive, reaching almost 200 m/yr. Downstream, the pattern is weaker and negative, -100 m/yr. The magnitude of the second-order pattern is an order of magnitude smaller than the first-order pattern, even in the upper glacier.

The second PC (Figure 8d) correlates significantly ($p = 0.008$) to the ice flow speed near the hinge point (cyan star in Figure 8b). The second PC peaks in mid July ($p < 10^{-6}$) and significantly correlates to runoff ($p < 10^{-3}$), but not to terminus position ($p = 0.4$), as shown in Figure 8e. Therefore, this mode is consistent with runoff-control. The second mode explains 2% of the variance in flow speed across the full domain, but approximately 10% of the variance upstream of the hinge point ~12 km from the terminus.

This test on Kangerlussuup Sermia demonstrates the validity of what Vijay et al. (2021) hypothesized: that ice flow is runoff-adapting in the lower glacier and runoff-driven farther upstream. Our EOF/PC analysis shows that the vast majority (95%) of the variance in ice flow speed over 2015–2021 on the entire glacier, however, is due to runoff-adapting behavior. Only 2% overall shows runoff-driven behavior.

4 Discussion

4.1 Benefits of EOF Analysis over Single-Point Analysis

Across all five glaciers we analyzed, the first mode captured a large majority of the variance in flow speed (70–95%, depending on the glacier) and was uniformly signed over nearly all of the domain for every glacier. This means that the inferred type is applicable over the entire domain, rather than just at the single, near-terminus point analyzed in previous studies. Helheim Glacier (Section 3.1) highlights this advantage, where the single-point flow speed correlates strongly with terminus position ($p < 10^{-16}$), yet the leading mode, which explains 95% of the variance in flow over the entire glacier, shows that both the terminus ($p < 10^{-4}$) and runoff volume ($p < 10^{-3}$) influence the speed domain-wide (Figure 4). The reduced correlation with terminus position underscores the fact that the first mode incorporates variability across the entire glacier domain, which extends nearly 50 km inland into regions that are unlikely to feel the influence of the terminus. Conversely, the single-point flow speed correlates much less, but still significantly, with runoff volume ($p = 0.02$), causing previous analyses to pass over runoff control in favor of terminus control (Vijay et al., 2019). In fact, runoff control is a strong secondary influence on flow speed over the entire Helheim Glacier domain ($r^2 = 0.15$, compared to $r^2 = 0.22$ for terminus position).

On Fenris Glacier, classification of the first PC yields runoff-adapting behavior ($p < 10^{-3}$, Section 3.2) with no hint of terminus control ($p = 0.4$), yet classification by the detrended speed at the single point near the terminus shows strong terminus control ($p < 10^{-13}$, Figure 5e). The first PC (Figure 5c) significantly correlates to the single-point speed (p=0.046), but it shows much higher interannual variability with a less clear seasonal cycle ($p < 10^{-3}$, peaking in May) than does the terminus position ($p < 10^{-7}$, peaking in September). As with Helheim Glacier, these observations imply that the flow variability farther from the terminus figures prominently in the first mode; single-point analyses miss this contribution.

Here we speculate reasons why the flow over the whole Fenris Glacier domain differs so much from flow at the single, near-terminus point. Fenris Glacier flows through a deep trough that reaches ~800 m below sea level near its terminus, allowing a strong marine influence and keeping the terminus lightly grounded since at least 2016 (Williams, n.d.). This should aid channelization in the subglacial environment, promoting runoff-adapting ice flow, as well as making ice flow more sensitive to terminus position (Kehrl et al., 2017). Farther upstream, ~25 km from the terminus, ice thickness reaches 1500 m yet with a steep surface gradient (~0.04), which should still allow channel formation and thus runoff-adapting behavior (Dow et al., 2014, 2015). At this distance, the effect of variations in terminus position on ice speed should decay greatly (I. Howat et al., 2005; Kehrl et al., 2017). Thus, we hypothesize that the first PC captures glacier-wide behavior, which tends to be runoff-adapting, rather than exclusively near-terminus behavior, as studied by Vijay et al. (2019), which is more strongly terminus-driven.

4.1.1 Utility for dual-type glaciers

On Kangerlussuup Sermia, our results show that the glacier is primarily runoff-adapting (95% of the variance in flow speed; Figure 8a, 8c), while the upper glacier (>12 km from the terminus) shows runoff-driven behavior. The runoff-driven mode only explains ~10% of the variance in the upper glacier, and 2% over the full domain (Figure 8b, 8d). This agrees with the Vijay et al. (2021) classification as runoff-adapting based on two points <10 km from the terminus, with runoff-driven behavior noted >15 km from the terminus. Our method delineates the transition point ~12 km from the terminus (Figure 8b) and also quantifies the strength of each type. This is a marked improvement over the previous, more qualitative analysis.

Our classification of Helheim Glacier as primarily terminus-driven and secondarily runoff-driven also likely points back to the advantage that EOF/PC analysis captures behavior across the entire domain, including the upper glacier where runoff control is more likely due to thicker ice and lower surface slopes that inhibit channelization (Dow et al., 2014, 2015). If this hypothesis that Helheim is a dual-type glacier holds, then Helheim differs from Kangerlussuup Sermia, where the two types appear in two different modes. In that case, Helheim would demonstrate that EOF / PC analysis does not always separate types into modes, and an additional step, such as independent component analysis (ICA), may be required to yield such separation.

4.1.2 Role of higher-order modes

EOF/PC decomposition of three years of glacier speed data in a 2.5 $\times$ 4 km area on Jakobshavn Isbræ by Ashmore et al. (2021) revealed similar results as we find here: a strong first mode (98%) followed by higher-order modes with coherent spatial and temporal patterns. However, Ashmore et al. (2021) discovered that modes 2 and 3 were paired: their PCs were highly correlated to one another, their EOFs were similar but shifted in space, and their eigenvalues had comparable values, in contrast to the eigenvalues of other modes, which followed a smooth exponential decline. We find something similar at Midgard Glacier: the eigenvalues of modes 2 and 3 have comparable values, rather than decline approximately exponentially as they do for the other glaciers we studied (Figure S1). Thus, we scrutinize modes 2 and 3 on Midgard Glacier to investigate the possibility of quasi-conjugate pairing as observed by Ashmore et al. (2021). Modes 2–3 for all glaciers appear in Figures S2–S6; those for Midgard Glacier are in Figure S4.

The second and third PCs on Midgard Glacier have no strong relationship to one another. The second PC shows a clear annual cycle peaking in mid-July ($p < 10^{-8}$), while the third PC shows no annual cycle ($p = 0.2$) or correlation with runoff ($p = 0.3$) or terminus position ($p = 0.3$). The second and third PCs also do not significantly correlate to one another ($p = 0.5$), in contrast with Ashmore et al. (2021). The second and third EOFs are more similar to each other than the PCs are, but their fundamental descriptions differ greatly. While the second EOF is primarily a dipole with an inflection point ~2 km from the terminus and secondarily separates the main trunk (negatively signed) from the eastern tributaries (positively signed), the third EOF separates the main trunk (negatively signed) from its immediate margins and only the easternmost of the tributaries (positively signed). This, too, is in contrast with Ashmore et al. (2021), who uncovered much more comparable EOFs than we find here.

Thus, we discard the hypothesis of quasi-conjugate pairing among these modes on our glaciers, even though this was observed on another glacier (Ashmore et al., 2021). We speculate that their smaller study area allowed their analysis to observe a traveling wave over their domain in consecutive modes, whereas our domains are too large to capture such a phenomenon. While traveling waves likely do occur on the Sermilik Fjord glaciers – e.g., from perturbations at the terminus or as the subglacial hydrologic system develops over a melt season – it is likely that analysis on a finer spatial scale would be required to observe these using EOF / PC tools.

4.2 Comparison to Previous Studies of Glacier Type

4.2.1 Helheim Glacier

At Helheim Glacier, Moon et al. (2014) observed both terminus control and runoff control in different years over 2009–2013 and, in some years, were unable to classify it at all. Vijay et al. (2019) interpreted Helheim as terminus-driven over 2015–2017. Our conclusion of terminus control over 2016–2021, with second-order runoff control, agrees well with these previous analyses. This is in contrast to Ultee et al. (2021), who concluded that on seasonal timescales, Helheim was primarily runoff-driven, and Bevan et al. (2015), who also found a link between runoff and seasonal surface elevation change.

If there is some runoff control at Helheim Glacier, this suggests that the subglacial hydrologic system remains inefficient through the melt season. Recent studies using subglacial modeling (Poinar et al., 2019; Sommers et al., 2022) and direct observations of plumes (Melton et al., 2022; Everett et al., 2016), however, suggest a seasonally channelized subglacial environment on the lower reach of Helheim Glacier. These conclusions are not necessarily inconsistent. Our analysis captures behavior across the entire domain, including the upper glacier where runoff-driven behavior is more likely, as discussed in Section 4.1.

An alternative explanation for our dual-type finding over 2016–2021 is that the type may vary from year to year. Indeed, Moon et al. (2014) found terminus control in 2009 and 2010, runoff control in 2009 and 2013, and was not able to classify its behavior in 2011 or 2012. During these time periods, the lowermost 5 km of Helheim Glacier was near flotation (Kehrl et al., 2017), which should make its velocity more sensitive to both terminus position and basal water volumes (Ultee et al., 2021). After 2015, the lower glacier was more consistently grounded (Roberts, 2018); this is the time period that both we and Vijay et al. (2019) study.

4.2.2 Fenris Glacier

Vijay et al. (2019) classified Fenris Glacier as terminus-driven in 2015–2017. Over that period, speeds on the glacier steadily increased (Figure 2). They declined briefly each autumn (Figure 5e) but reached a new peak near the beginning of each melt season. During the 2019 melt season, the terminus retreated continuously $\sim$3 km upfjord to its shortest position in the observational record to date (Goliber et al., 2022), which may explain its apparent terminus-driven behavior, and lack of runoff-adapting behavior, that year. Indeed, if the long-term trend is retained in the terminus and single-point speed time series, there is significant correlation that suggests terminus control over the long term; this is the nature of the Vijay et al. (2019) analysis. However, when the long-term trend is removed, as we do here, what remains is runoff-adapting behavior on the seasonal scale.

Alternately, the discrepancy in type could be due to the different time interval if Fenris changed its type sometime between 2017 and 2021, or because Fenris as a whole behaves as runoff-adapting, while the point analyzed by Vijay et al. (2019) responds to terminus position more strongly than points around it. If the latter is true, this points to the necessity of pan-spatial analyses, such as EOF/PC analysis, to capture the full behavior of the glacier.

4.2.3 Midgard Glacier

Vijay et al. (2019, 2021) classified Midgard Glacier as runoff-adapting over 2015–2019. Our analysis over 2016–2021 agrees. Over these periods, the speed of Midgard Glacier did not substantially change; in fact, it decreased slightly. The terminus did retreat significantly while still showing a strong seasonal cycle. Thus, for this glacier, results from our analysis that isolates seasonal signals should and do agree with those from the Vijay et al. (2019, 2021) method that includes any long-term trends.

4.2.4 Pourquoi Pas Glacier

Vijay et al. (2019) classified Pourquoi Pas Glacier as terminus-driven over 2015–2017, in contrast with our conclusion of runoff-driven. Similarly to Fenris Glacier, they reached this classification by correlating the long-term trends in velocity and terminus position. (Long-term trends in runoff were, predictably, much smaller.) The Vijay et al. (2019) data show no strong seasonal cycle in terminus position on Pourquoi Pas Glacier over 2015–2017, but rather a longer-term retreat that began in 2016 and coincided with a speedup. As on Fenris Glacier, when the long-term trends in velocity and terminus position are removed, the controlling seasonal pattern of ice flow emerges, here as runoff-controlled.

4.3 Potential controls on glacier type

There are currently multiple hypotheses regarding what controls the seasonal flow type of a glacier. These are largely sortable as "geometric" (e.g., Davison et al., 2020) and "geographic" (e.g., Vijay et al., 2021).

Davison et al. (2020) make the case that larger outlet glaciers, which tend to be more lightly grounded than smaller glaciers, should be more likely to be terminus-driven. This hypothesis is supported by other studies of large outlet glaciers (e.g., I. Howat et al., 2005; Kehrl et al., 2017) and is also consistent with our results: Helheim Glacier, which has an annual flux of $\sim$29 Gton/yr (Mankoff et al., 2019) shows terminus control, while Midgard Glacier ($\sim$3.2 Gton/yr), Fenris Glacier ($\sim$2.6 Gton/yr), and Pourquoi Pas Glacier (too small to be analyzed by Mankoff et al., 2019) do not. The moderately-sized Fenris and Midgard Glaciers are both runoff-adapting, while the smaller Pourquoi Pas Glacier is runoff-driven. These three glaciers have similar surface slopes (I. M. Howat et al., 2014; I. Howat et al., 2022), which should imply that the runoff-driven Pourquoi Pas has thicker ice that is more of a hindrance to channelization than the other two glaciers (Dow et al., 2014, 2015). However, ice thickness at Pourquoi Pas Glacier rarely exceeds $\sim$100 m (Morlighem, 2021), while it locally exceeds 1000 m in the center of the Fenris and Midgard Glacier troughs. This discrepancy may be due to inaccurate bed information for Pourquoi Pas Glacier: the data there were derived from kriging and interpolation, while for Fenris and Midgard Glaciers, the more accurate mass conservation method was used (Morlighem, 2021; Morlighem et al., 2017). For a speed of 200 m/yr (Figure 2), ice temperature -10°C, and a typical local surface slope of 0.04, Glen's Flow Law suggests an ice thickness of $\sim$1000 m near the terminus of Pourquoi Pas Glacier. This would be comparable to that of Fenris and Midgard Glaciers, which have a different type. Overall, the geometric argument, that glacier size and shape is predictive of its type, performs imperfectly in Sermilik Fjord because of Pourquoi Pas Glacier.

Vijay et al. (2021) noticed a geographic trend of runoff-driven glaciers in the north ($\gtrsim$ 78°N latitude) and runoff-adapting glaciers in the south ($\lesssim$ 72°N latitude). This, too, is imperfect; some 20% of northern glaciers in the (Vijay et al., 2021)study were runoff-adapting, and a similar percent of southern glaciers were runoff-driven. Furthermore, Sakakibara and Sugiyama (2019) noted runoff-adapting behavior in at least 7 of the 10 glaciers they studied in Prudhoe Land ($\sim$ 78°N latitude), which is inconsistent with the broad Vijay et al. (2021) hypothesis. As in other studies, the strength of runoff-control versus runoff-adapting signal varied between even neighboring glaciers studied by Sakakibara and Sugiyama (2019). We find the same effect in Sermilik Fjord: four glaciers within a 100 km span, touching the same fjord ocean boundary condition, show all three types of seasonal ice flow. While there may be a suggestion of an east-west gradient in glacier type, it is weak, especially as Midgard Glacier (runoff-adapting) and Pourquoi Pas Glacier (runoff-driven) have termini $\sim$3 km apart and were tributaries of a common glacier as recently as 2011 (Korsgaard, 2021). However, our study of four nearby glaciers is inadequate to test the island-scale hypothesis of Vijay et al. (2021); thus, we only submit a lack of evidence in favor of the geographic hypothesis, not a rejection of it.

5 Conclusion

Our use of EOF / PC analysis to decompose glacier flow type uncovers all three types in Sermilik Fjord: ice flow in Helheim Glacier is primarily terminus-driven, ice flow in Fenris and Midgard Glaciers is runoff-adapting, and ice flow in Pourquoi Pas Glacier is runoff-driven. We also find that Helheim and Midgard Glaciers have secondary runoff-driven types, and that Kangerdlussuup Sermia in western Greenland has two types that are separate in space. We find evidence that glacier geometry, including the ice flux magnitude, ice thickness, and surface slope, is predictive of its flow type, as previously hypothesized, but the fit is imperfect across Sermilik Fjord.

Our primary types differ slightly from previous work because we isolate seasonal patterns, unlike Vijay et al. (2019, 2021), and because we consider ice flow across large glacier domains (150–350 km^2) that allow contributions from the mid-trunk, sidewalls, and upper tributaries, unlike previous work that exclusively analyzed the near-terminus area. With today's widely available and spatially comprehensive datasets for ice flow speed across hundreds of glaciers in Greenland, Antarctica, and mountain environments worldwide, the typical inclusion of EOF / PC tools in standard analysis packages, and the relatively fast run-time of these algorithms, we suggest the use of wider spatial analysis tools, such as EOF / PC analysis, for assessment of glacier flow type.

Open Research Statement

All velocity data analyzed is publicly available at the NSIDC, as referenced. Terminus positions generated for this study, as well as the selected ice speed data and EOF/PC results, are available at `http://hdl.handle.net/10477/84288`.

Acknowledgments

The Heising-Simons Foundation, Grant #2020-1910, supported this work. I thank Matt Knepley and Stuart Evans for useful conversations about EOF/PC analysis. This work stemmed from a classroom example I developed to teach the execution and interpretation of EOF/PC analysis in earth science.

References

Ashmore, D. W., Mair, D. W. F., Higham, J. E., Brough, S., Lea, J. M., & Nias, I. J. (2021). Proper orthogonal decomposition of ice velocity identifies drivers of flow variability at Sermeq Kujalleq (Jakobshavn Isbræ). *The Cryosphere*, *16*(1), 219–236. doi: 10.5194/tc-16-219-2022

Bevan, S. L., Luckman, A., Khan, S. A., & Murray, T. (2015). Seasonal dynamic thinning at Helheim Glacier. *Earth and Planetary Science Letters*, *415*(C), 47 – 53. doi: 10.1016/j.epsl.2015.01.031

Bjørk, A. A., Aagaard, S., Lütt, A., Khan, S. A., Box, J. E., Kjeldsen, K. K., … Kjær, K. H. (2018). Changes in Greenland's peripheral glaciers linked to the North Atlantic Oscillation. *Nature Climate Change*, *8*(1), 48–52. doi: 10.1038/s41558-017-0029-1

Bjørk, A. A., Kruse, L. M., & Michaelsen, P. B. (2015). Brief communication: Getting Greenland's glaciers right – a new data set of all official Greenlandic glacier names. *The Cryosphere*, *9*(6), 2215–2218. doi: 10.5194/tc-9-2215-2015

Campbell, A. J., Hulbe, C. L., & Lee, C.-K. (2017). The shape of change: an EOF approach to identifying sources of transient thickness change in an ice shelf. *doi.org*, 1 – 7. doi: 10.1017/aog.2017.16

Cheng, D., Hayes, W., Larour, E., Mohajerani, Y., Wood, M., Velicogna, I., & Rignot, E. (2021). Calving Front Machine (CALFIN): glacial termini dataset and automated deep learning extraction method for Greenland, 1972–2019. *The Cryosphere*, *15*(3), 1663–1675. doi: 10.5194/tc-15-1663-2021

Csathó, B. M., Schenk, A. F., Veen, C. J. v. d., Babonis, G., Duncan, K., Rezvanbehbahani, S., … Angelen, J. H. v. (2014). Laser altimetry reveals complex pattern of Greenland Ice Sheet dynamics. *Proceedings of the National Academy of Sciences of the United States of America*. doi: 10.1073/pnas.1411680112

Davison, B. J., Sole, A. J., Cowton, T. R., Lea, J. M., Slater, D. A., Fahrner, D., & Nienow, P. W. (2020). Subglacial Drainage Evolution Modulates Seasonal Ice Flow Variability of Three Tidewater Glaciers in Southwest Greenland. *Journal of Geophysical Research: Earth Surface*, *125*(9). doi: 10.1029/2019jf005492

Dow, C. F., Kulessa, B., Rutt, I. C., Doyle, S. H., & Hubbard, A. (2014). Upper bounds on subglacial channel development for interior regions of the Greenland ice sheet. *Journal of Glaciology*, *60*(224), 1044 – 1052. doi: 10.3189/2014jog14j093

Dow, C. F., Kulessa, B., Rutt, I. C., Tsai, V. C., Pimentel, S., Doyle, S. H., … Hubbard, A. (2015). Modeling of subglacial hydrological development following rapid supraglacial lake drainage. *Journal of Geophysical Research: Earth Surface*, *120*(6), 1127 – 1147. doi: 10.1002/2014jf003333

Everett, A., Murray, T., Selmes, N., Rutt, I. C., Luckman, A., James, T. D., … Reeve, D. E. (2016). Annual down-glacier drainage of lakes and water-filled crevasses at Helheim Glacier, southeast Greenland. *Journal of Geophysical Research: Earth Surface*, *121*(10), 1819 – 1833. doi: 10.1002/2016jf003831

Felikson, D., Nowicki, S., Nias, I., Morlighem, M., & Seroussi, H. (2022). Seasonal Tidewater Glacier Terminus Oscillations Bias Multi-Decadal Projections of Ice Mass Change. *Journal of Geophysical Research: Earth Surface*, *127*(2). doi: 10.1029/2021jf006249

Goliber, S., Black, T., Catania, G., Lea, J. M., Olsen, H., Cheng, D., … Zhang, E. (2022). TermPicks: a century of Greenland glacier terminus data for use in scientific and machine learning applications. *The Cryosphere*, *16*(8), 3215–3233. doi: 10.5194/tc-16-3215-2022

Gregson, J. (1995). Probing the Pourquoi-Pas: The Karabiner Mountaineering Club Greenland Expedition 1994. *The Alpine Journal*, 183–192. Retrieved from `https://www.alpinejournal.org.uk/Contents/Contents\_1995\_files/AJ\%201995\%20183-192\%20Gregson\%20Greenland.pdf`

Howat. (2020). MEaSUREs Greenland Ice Velocity Selected Glacier Site Velocity Maps from Optical Images, Version 3. *NASA National Snow and Ice Data Center Distributed Active Archive Center*. doi: 10.5067/rrfy5iw94x5w

Howat, I., Joughin, I., Tulaczyk, S., & Gogineni, S. (2005). Rapid retreat and acceleration of Helheim Glacier, east Greenland. *Geophysical Research Letters*, *32*(22). doi: 10.1029/2005gl024737

Howat, I., Negrete, A., & Smith, B. (2022). MEaSUREs Greenland Ice Mapping Project (GrIMP) Digital Elevation Model from GeoEye and WorldView Imagery, Version 2. *NASA National Snow and Ice Data Center Distributed Active Archive Center*. doi: 10.5067/bhs4s5gamfvy

Howat, I. M., Box, J. E., Ahn, Y., Herrington, A., & McFadden, E. M. (2010). Seasonal variability in the dynamics of marine-terminating outlet glaciers in Greenland. *Journal of Glaciology*, *56*(198), 601–613. doi: 10.3189/002214310793146232

Howat, I. M., Negrete, A., & Smith, B. E. (2014). The Greenland Ice Mapping Project (GIMP) land classification and surface elevation data sets. *The Cryosphere*, *8*(4), 1509 – 1518. doi: 10.5194/tc-8-1509-2014

Iken, A., & Bindschadler, R. A. (1986). Combined measurements of Subglacial Water Pressure and Surface Velocity of Findelengletscher, Switzerland: Conclusions about Drainage System and Sliding Mechanism. *Journal of Glaciology*, *32*(110), 101 – 119. doi: 10.3189/s0022143000006936

Joughin, I. (2021). MEaSUREs Greenland Monthly Ice Sheet Velocity Mosaics from SAR and Landsat, Version 3. *NASA National Snow and Ice Data Center Distributed Active Archive Center*. doi: 10.5067/ydlh5qg02xkc

Joughin, I., Howat, I., Smith, B., & Scambos, T. (2021). MEaSUREs Greenland Ice Velocity Selected Glacier Site Velocity Maps from InSAR, Version 4. *NASA National Snow and Ice Data Center Distributed Active Archive Center*. doi: 10.5067/gqzqy2m5507z

Joughin, I., Shean, D. E., Smith, B. E., & Floricioiu, D. (2019). A Decade of Variability on Jakobshavn Isbrae: Ocean Temperatures Pace Speed Through Influence on Mélange Rigidity. *The Cryosphere*, 1 – 27. doi: 10.5194/tc-2019-197

Joughin, I., Smith, B. E., & Howat, I. (2018). Greenland Ice Mapping Project: ice flow velocity variation at sub-monthly to decadal timescales. *The Cryosphere*, *12*(7), 2211 – 2227. doi: 10.5194/tc-12-2211-2018

Joughin, I., Smith, B. E., Howat, I. M., Floricioiu, D., Alley, R. B., Truffer, M., & Fahnestock, M. (2012). Seasonal to decadal scale variations in the surface velocity of Jakobshavn Isbrae, Greenland: Observation and model-based analysis. *Journal of Geophysical Research: Solid Earth*, *117*(F2), 1 – 20. doi: 10.1029/2011jf002110

Joughin, I., Smith, B. E., Howat, I. M., Scambos, T., & Moon, T. (2010). Greenland flow variability from ice-sheet-wide velocity mapping. *Journal of Glaciology*, *56*(197), 415 – 430.

Kehrl, L. M., Kehrl, L. M., Joughin, I., Shean, D. E., Shean, D. E., Floricioiu, D., & Krieger, L. (2017). Seasonal and interannual variabilities in terminus position, glacier velocity, and surface elevation at Helheim and Kangerlussuaq Glaciers from 2008 to 2016. *Journal of Geophysical Research: Earth Surface*, *122*(9), 1635 – 1652. doi: 10.1002/2016jf004133

King, M. D., Howat, I. M., Candela, S. G., Noh, M. J., Jeong, S., Noël, B. P. Y., ... Negrete, A. (2020). Dynamic ice loss from the Greenland Ice Sheet driven by sustained glacier retreat. *Communications Earth & Environment*. doi: 10.1038/s43247-020-0001-2

Korsgaard, N. (2021). Greenland Ice Sheet outlet glacier terminus positions 1978-1987 from aero-photogrammetric map data. *GEUS Dataverse*. doi: 10.22008/fk2/b2jyvc

Lea, J. M. (2018). The Google Earth Engine Digitisation Tool (GEEDiT) and the Margin change Quantification Tool (MaQiT) – simple tools for the rapid mapping and quantification of changing Earth surface margins. *Earth Surface Dynamics*, *6*(3), 551 – 561. doi: 10.5194/esurf-6-551-2018

Lemos, A., Shepherd, A., McMillan, M., Hogg, A. E., Hatton, E., & Joughin, I. (2018). Ice velocity of Jakobshavn Isbræ, Petermann Glacier, Nioghalvfjerdsfjorden and Zachariæ Isstrøm, 2015-2017, from Sentinel 1-a/b SAR imagery. *The Cryosphere*, 1 – 18. doi: 10.5194/tc-2017-251

Lorenz, E. (1951). Seasonal and irregular variations of the Northern Hemisphere sea-level pressure profile. *Journal of Meteorology*, *8*(1), 52–59. doi: 10.1175/1520-0469(1951)008⟨0052:saivot⟩2.0.co;2

Lorenz, E. (1956). Empirical Orthogonal Functions and Statistical Weather Prediction.

MacGregor, J. A., Fahnestock, M. A., Colgan, W. T., Larsen, N. K., Kjeldsen, K. K., & Welker, J. M. (2020). The age of surface-exposed ice along the northern margin of the Greenland Ice Sheet. *Journal of Glaciology*, *66*(258), 667 – 684. doi: 10.1017/jog.2020.62

Mair, D. (2002). Influence of subglacial drainage system evolution on glacier surface motion: Haut Glacier d'Arolla, Switzerland. *Journal of Geophysical Research*, *107*(B8), 308 – 13. doi: 10.1029/2001jb000514

Mankoff, K. D., Colgan, W., Solgaard, A., Karlsson, N. B., Ahlstrøm, A. P., As, D. V., . . . Fausto, R. S. (2019). Greenland Ice Sheet discharge from 2000 to 2018. *Earth System Science Data*, 1 – 31. doi: 10.5194/essd-11-769-2019

Mantelli, E., Bertagni, M. B., & Ridolfi, L. (2016). Stochastic ice stream dynamics. *Proceedings of the National Academy of Sciences*, *113*(32), E4594–E4600. doi: 10.1073/pnas.1600362113

Melton, S. M., Alley, R. B., Anandakrishnan, S., Parizek, B. R., Shahin, M. G., Stearns, L. A., . . . Finnegan, D. C. (2022). Meltwater drainage and iceberg calving observed in high-spatiotemporal resolution at Helheim Glacier, Greenland. *Journal of Glaciology*, 1–17. doi: 10.1017/jog.2021.141

Mishra, V., Smoliak, B. V., Lettenmaier, D. P., & Wallace, J. M. (2012). A prominent pattern of year-to-year variability in Indian Summer Monsoon Rainfall. *Proceedings of the National Academy of Sciences*, *109*(19), 7213–7217. doi: 10.1073/pnas.1119150109

Moon, T., Joughin, I., Smith, B., Broeke, M. R. v. d., Berg, W. J. v. d., Noel, B., & Usher, M. (2014). Distinct patterns of seasonal Greenland glacier velocity. *Geophysical Research Letters*, *41*(20), 7209 – 7216. doi: 10.1002/2014gl061836

Morlighem, M. (2021). IceBridge BedMachine Greenland, Version 4. *NASA National Snow and Ice Data Center Distributed Active Archive Center*. doi: 10.5067/vlj5yxkcngxo

Morlighem, M., Williams, C. N., Rignot, E., An, L., Arndt, J. E., Bamber, J. L., . . . Zinglersen, K. B. (2017). BedMachine v3: Complete Bed Topography and Ocean Bathymetry Mapping of Greenland From Multibeam Echo Sounding Combined With Mass Conservation. *Geophysical Research Letters*, *44*(21), 11,051 – 11,061.

Mouginot, J., Rignot, E., Bjørk, A. A., Broeke, M. V. d., Millan, R., Morlighem, M., . . . Wood, M. (2019). Forty-six years of Greenland Ice Sheet mass balance from 1972 to 2018. *Proceedings of the National Academy of Sciences*, *78*. doi: 10.1073/pnas.1904242116

Poinar, K., & Andrews, L. C. (2021). Challenges in predicting Greenland supraglacial lake drainages at the regional scale. *The Cryosphere*, *15*(3), 1455–1483. doi: 10.5194/tc-15-1455-2021

Poinar, K., Dow, C. F., & Andrews, L. C. (2019). Long-Term Support of an Active Subglacial Hydrologic System in Southeast Greenland by Firn Aquifers. *Geophysical Research Letters*, *57*(204), 609 – 619. doi: 10.1029/2019gl082786

Rienecker, M. M., Suarez, M. J., Gelaro, R., Todling, R., Bacmeister, J., Liu, E., . . .

Woollen, J. (2011). MERRA: NASA's Modern-Era Retrospective Analysis for Research and Applications. *Journal of Climate*, *24*(14), 3624 – 3648. doi: 10.1175/jcli-d-11-00015.1

Roberts, C. (2018). *Hydrologic Controls on Ice Dynamics Inferred at Helheim Glacier, Southeast Greenland, from High-Resolution Surface-Elevation Record* (Unpublished doctoral dissertation).

Sakakibara, D., & Sugiyama, S. (2019). Seasonal ice-speed variations in 10 marine-terminating outlet glaciers along the coast of Prudhoe Land, northwestern Greenland. *Journal of Glaciology*. doi: 10.1017/jog.2019.81

Smoliak, B. V., & Wallace, J. M. (2015). On the Leading Patterns of Northern Hemisphere Sea Level Pressure Variability*. *Journal of the Atmospheric Sciences*, *72*(9), 3469–3486. doi: 10.1175/jas-d-14-0371.1

Sommers, A., Meyer, C., Morlighem, M., Rajaram, H., Poinar, K., Chu, W., & Mejia, J. (2022). Subglacial hydrology modeling predicts high winter water pressure and spatially variable transmissivity at Helheim Glacier, Greenland. *Journal of Glaciology*, 1–33.

Thompson, D. W. J., & Wallace, J. M. (1998). The Arctic oscillation signature in the wintertime geopotential height and temperature fields. *Geophysical Research Letters*, *25*(9), 1297–1300. doi: 10.1029/98gl00950

Ultee, L., Felikson, D., Minchew, B., Stearns, L. A., & Riel, B. (2021). Statistical inference of the ice velocity response to meltwater runoff, terminus position, and bed topography at Helheim Glacier, Greenland. doi: 10.1002/essoar.10506878.1

Vijay, S., Khan, S. A., Kusk, A., Solgaard, A. M., Moon, T., & Bjørk, A. A. (2019). Resolving Seasonal Ice Velocity of 45 Greenlandic Glaciers With Very High Temporal Details. *Geophysical Research Letters*, *46*(3), 1485 – 1495. doi: 10.1029/2018gl081503

Vijay, S., King, M. D., Howat, I. M., Solgaard, A. M., Khan, S. A., & Noël, B. (2021). Greenland ice-sheet wide glacier classification based on two distinct seasonal ice velocity behaviors. *Journal of Glaciology*, *67*(266), 1241–1248. doi: 10.1017/jog.2021.89

Walsh, K., Howat, I. M., Ahn, Y., & Enderlin, E. M. (2012). Changes in the marine-terminating glaciers of central east Greenland, 2000–2010. *The Cryosphere*, *6*(1), 211 – 220. doi: 10.5194/tc-6-211-2012

Wilks, D. S. (2019). *Statistical Methods in the Atmospheric Sciences.* Elsevier. Retrieved from `https://www.elsevier.com/books/statistical-methods-in-the-atmospheric-sciences/wilks/978-0-12-815823-4` doi: 10.1016/c2017-0-03921-6

Williams. (n.d.). *Controls on ice dynamics of the Greenland Ice Sheet* (Unpublished doctoral dissertation).